Nonlinearity from stress corrosion cracking as a function of chloride exposure time using the time reversed elastic nonlinearity diagnostic

Sarah M. Young, Brian E. Anderson, Stephen M. Hogg, Pierre-Yves Le Bas, and Marcel C. Remillieux

Nonlinearity from stress corrosion cracking as a function of chloride exposure time using the time reversed elastic nonlinearity diagnostic

Sarah M. Young,[1] Brian E. Anderson,[1,a)] Stephen M. Hogg,[1] Pierre-Yves Le Bas,[2] and Marcel C. Remillieux[3]

[1]*Acoustics Research Group, Department of Physics and Astronomy, Brigham Young University, N283 Eyring Science Center, Provo, Utah 84602, USA*

[2]*Detonation Science and Technology Group (Q-6), Los Alamos National Laboratory, MS C925, Los Alamos, New Mexico 87545, USA*

[3]*Geophysics Group (EES-17), Los Alamos National Laboratory, MS D446, Los Alamos, New Mexico 87545, USA*

The Time Reversed Elastic Nonlinearity Diagnostic (TREND) has a long history of successful non-destructive detection of cracks in solids using nonlinear indicators. Recent research implemented TREND to find stress corrosion cracking (SCC) in the heat-affected zone adjacent to welds in stainless steel. SCC development around welds is likely to occur due to the temperature and chemical exposure of steel canisters housing spent nuclear fuel. The ideal SCC detection technique would quantify the size and extent of the SCC, rather than just locating it, as TREND has been used for in the past. The current paper explores TREND's ability to detect an assumed increase in SCC over time using 13 samples exposed to a magnesium chloride ($MgCl_2$) bath for different lengths of time. The samples are then scanned with TREND and nonlinearity is quantified for each scan point and each sample. The results suggest that TREND can be used to not only locate SCC in the heat-affected zone, but also track an increase in nonlinearity, and thereby an increase in damage, in samples exposed to the $MgCl_2$ solution for a longer duration. © 2019 Acoustical Society of America.
https://doi.org/10.1121/1.5087828

I. INTRODUCTION

Time reversal (TR) focusing has been used for the nondestructive evaluation (NDE) of solid media for just over a decade. TR utilizes the reversed impulse response of a system to generate a temporal focus of vibration energy at a single location,[1] which can be used to reveal the local system properties upon examination of the focal signal.[2] Direct excitation of a cracked location may be insufficient for generation of the amplitudes necessary to allow detection of the nonlinear response of the damage. TR focusing has been shown to generate 30 times higher peak amplitude than direct excitation (though a factor of about 10 is typical), per channel, and therefore has sufficient amplitude to allow detection of local nonlinear properties.[3] Analysis of the TR focal signal reveals nonlinear variations in a number of forms including higher signal amplitude, waveform distortions,[4,5] or nonlinear harmonic content.[6,7] For a focus at a cracked location in a medium, all of these indicators and more typically exist.

The earliest methods utilizing TR for NDE detected scattered waves from a defect as an impulse response that could then be reversed in time and focused at the defect to localize it.[8–11] This linear process, called DORT (for the decomposition of the time reversal operator), was used for flaw detection in materials such as titanium and duralumin.[12–15] An iterative

TR technique was also developed to increase the scattered signal strength.[16,17] In solid media, additional linear TR methods have been developed to locate acoustic emissions,[18,19] earthquakes,[20–23] finger taps,[24,25] and linear scatterers.[26–28] The use of TR for the nonlinear detection of cracks was proposed by Guyer[29] and numerically verified by Delsanto *et al.*[30] and Bou Matar *et al.*[31] Sutin *et al.*[6,7] were able to experimentally confirm a reciprocal TR process where a focus is placed at any location specified by a noncontact receiver, allowing an entire region to be studied without transducer rebonding. Experimental validation of the use of TR for nonlinear detection and imaging of cracks was done for impact damage[32,33] as well as stress fatigue[34] and delaminations.[35,36] In these studies, high-amplitude TR focusing was intentionally used to excite local nonlinearities from damage, and ultimately, a technique termed the Time Reversed Elastic Nonlinearity Diagnostic (TREND) was developed to image damage in a sample.[36–38] Additional recent experiments have used nonlinear techniques in conjunction with TR to study closed cracks,[39] and use TREND to both locate and study the depth of stress corrosion cracking (SCC) near welds.[40–42] An overview and summary of TR techniques for NDE utilizing nonlinear acoustics was recently published.[43]

The TREND technique excites nonlinearities at a specific location by training a high amplitude TR focus of acoustic energy to that location. A series of scan points is selected in a region of interest and a TR focus is generated

a)Electronic mail: bea@byu.edu

and measured at each location in turn. In these experiments, the TR focus of energy at a single location, even a cracked one, is still considered to be nondestructive since the strain is kept at least an order of magnitude smaller than the linear strain relationships of the undamaged medium. By evaluating each scan point's focal signal for nonlinear content, a visual map of the quantified nonlinear signature is produced wherein high amounts of nonlinearity are assumed to imply more damage. Because every hardware system inherently generates some level of nonlinearity, assessments of nonlinearity correlated to damage should be made relative to a measurement at an undamaged location in the sample or to an undamaged sample. This relies on a clear distinction between system and sample nonlinearity, a sometimes difficult requirement not always necessary for linear detection systems. The success of TREND is partially due to its localized, high focal amplitude, which makes system noise less of a problem. In addition, studies have shown that nonlinear detection methods like TREND are able to find damage at a very early stage,[44] as opposed to linear acoustic techniques (e.g., pulse echo) that tend to detect the damage once the system is close to failure.

Recent research investigated the use of TREND for non-destructive localization and characterization of SCC with application to steel canisters holding spent nuclear fuel.[40,42,45] The approximately 3.7 m (12 ft) diameter cylindrical canisters are air-tight and are surrounded by a cylindrical concrete cask with air vents. These canisters are often stored near coastlines. Due to internal heating and a cool exterior, the salt-air exposure, and residual stresses, SCC may develop near welds. Long exposure to these conditions might lead to SCC beginning to threaten the air-tight seal.[46–48]

The development of SCC around welds occurs as a result of residual stress and long-term exposure to moist, chloridic environments.[49] In austenitic stainless steels, like those used for nuclear fuel storage canisters, the necessarily high heat associated with the welding process adjusts the structure of the steel adjacent to the weld, allowing the base steel to bond to the weld filler material, but also potentially weakening the crystalline framework of the base steel. The steel altered by the heat of welding is called the Heat-Affected Zone (HAZ). After cooling, the HAZ can often be roughly identified by external discoloration caused by oxidation of the steel adjacent to the weld,[50] although it is impossible to know the true extent of the HAZ without high resolution imaging of the grain structure.[51] Within the HAZ, the grain boundaries at the transition between the base and filler metals can result in a residual stress from the welding process. Given ongoing exposure to high temperatures, humidity, chlorides, or any service-induced stress, SCC is most likely to form within the HAZ, especially along the edge of the weld.[42,49] An example of SCC in stainless steel is shown in Fig. 1 with labels indicating the weld, HAZ, and SCC.

In the study conducted by Anderson et al.,[40] a sample of 304L stainless steel (the subject of the photograph in Fig. 1), the same steel used in the storage canisters, was welded and subject to a boiling magnesium chloride ($MgCl_2$) bath to induce SCC in the HAZ. Imaging nonlinearity along the weld with TREND identified not only the location of SCC,
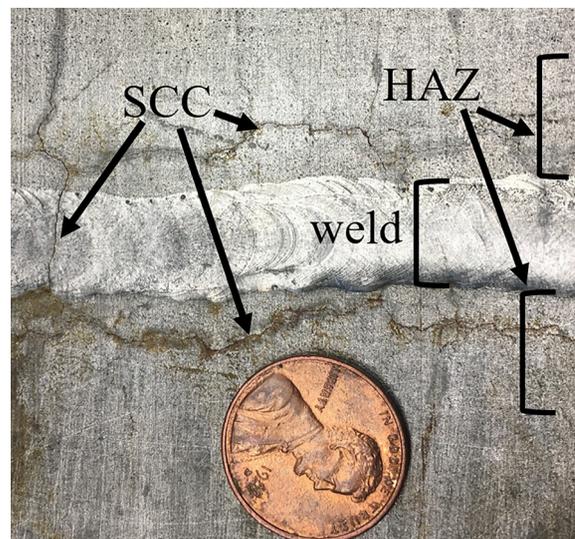

FIG. 1. (Color online) An image of 304L stainless steel with SCC in the HAZ just outside the weld. In this case, SCC has developed in the HAZ and occasionally in the weld.

but also discovered clues concerning the depth dependence of the cracking by using various frequency bandwidths for measurement. The external concrete encasing the steel canisters makes inspection difficult, but the TREND method may be employed in the intentional gap (for air flow) left between the steel canister and concrete cask making it possible to inspect SCC without disturbing the protective barriers.

A number of other nonlinear ultrasound techniques aimed at NDE of SCC have been used in the past. Ohara et al.[52] used a Subharmonic Phased Array to detect frequency mixing by SCC on the opposite side of a sample from the transducer or on the same side of the sample.[53] Dynamic Acousto-Elastic Testing was used to compare time-of-flight measurements across a dynamically strained crack.[54] Nonlinear Resonant Ultrasound Spectroscopy was used to locate SCC from resonance frequency shifts observed for different modes of a globally excited sample.[55] Morlock et al.[56] used Rayleigh waves to excite SCC which are then detected downstream of the crack. This last experiment was the only one to use multiple samples with differing degrees of SCC, which were induced by applying differing amounts of stress to samples exposed to a corrosive environment for the same amount of time. So far, there has not been a published study that exposed several samples to a corrosive environment for differing amounts of time nor a study exposing one sample to corrosion, monitoring it, and then exposing it again and repeating this cycle. This work does the former, exposing multiple samples to corrosion for differing amounts of time. Some of the above techniques were designed for advanced laboratory studies and not for field work (e.g., Dynamic Acousto-Elastic Testing), and some cannot easily localize SCC (e.g., Nonlinear Resonant Ultrasound Spectroscopy).

Developing TREND to be a robust tool for detecting and imaging of SCC for field testing is desired, meaning the ability to detect the depth of SCC and the orientation of the SCC. This information could allow corrective action to be taken before the air-tight seal is compromised. The purpose

of this paper is to experimentally study the ability of TREND to locate SCC in the HAZ of welds, but more importantly, correlate the amount of measured nonlinearity to the assumed amount of SCC present. By exposing a number of identically welded steel samples to a hot $MgCl_2$ solution for varying amounts of time, a series of samples are created with an expected, successive increase in SCC with longer exposure time. Using TREND, each of these samples is nondestructively examined and it is found that, with some variation, the longer a sample is exposed to the solution of $MgCl_2$, the more nonlinearity is measured in the HAZ.

The paper first describes the details of TREND processing, including the details of the system used, and experimental specifications. This will be followed by a description of the samples as well as the process for inducing SCC in the HAZ of each sample. Results of nonlinear imaging of cracks will be shown in detail for a representative sample after which the overall nonlinearity for each sample will be calculated and plotted against the exposure time of the sample to the hot $MgCl_2$ solution.

II. EXPERIMENTAL SETUP

TR utilizes the impulse response between a source and receiver to create a focus of energy at a selected location.[1,2] In the so called forward propagation step, an acoustic impulse is sent from a source, which propagates throughout the medium including multiple reflections and scattering, and is recorded by a receiver as the impulse response. In standard TR, the impulse response is reversed in time and emitted from the original receiver location. In this backward propagation step, the emitted waves constructively interfere to generate a focus of acoustic energy at the original location of the source during the forward step. If reciprocity can be assumed in the medium, the time-reversed impulse response can instead be emitted from the source location during the backward step to generate a focus at the receiver location. This method is termed reciprocal TR and utilizes the convenience of a source emitter that remains in place during the forward and backward steps.[57,58] In applying reciprocal TR to nonlinear detection of damage, a non-contact receiver allows a system to be trained to focus at multiple locations without moving the sources and provides a simple and quick method for imaging nonlinearity.

A PSV-400 Polytec (Waldbronn, Germany) scanning laser Doppler vibrometer (SLDV) provides a noncontact receiver to measure out-of-plane velocity on the sample surface and eight piezoelectric transducers (from APC International located in Mackeyville, PA, material type 850), measuring 19.0 mm in diameter by 12.0 mm in thickness, generate the source signals. In practice, a truly impulsive waveform is difficult to generate with band-limited piezoelectric transducers. Therefore, a linear chirp signal, like that shown in Fig. 2(a) (where the frequency content has been altered for visualization purposes), is utilized as the source signal for the forward propagation step, and a chirp response, shown in Fig. 2(b), is collected at the receiver in lieu of an impulse response.[59,60] The chirp signal is cross correlated with the chirp response in order to determine the required
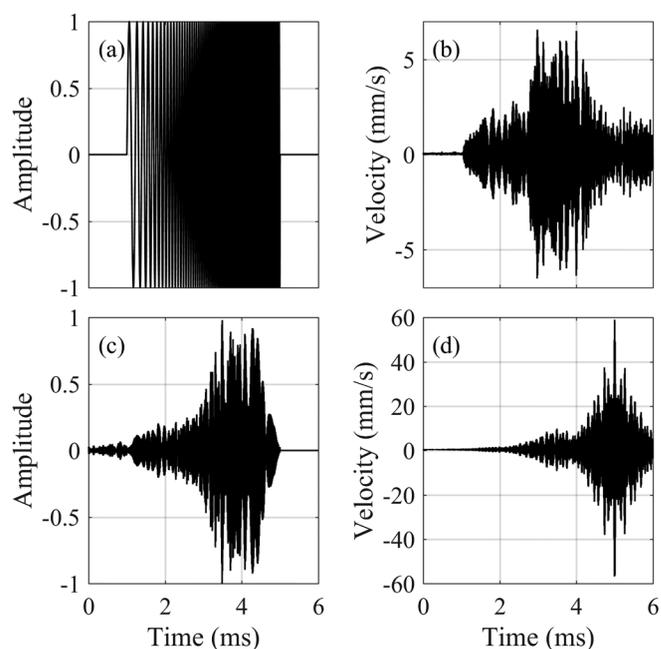

FIG. 2. Example signals used in the time reversal process for the given experiments. (a) Normalized chirp signal used as the initial source excitation (the frequencies shown are intentionally decreased for visualization purposes). (b) Normalized chirp response, measured at the receiver location. (c) Normalized reversed impulse response, generated by a cross correlation of (a) and (b). (d) Focal signal generated at the receiver location.

reversed impulse response [see Fig. 2(c)]. The reversed impulse response is sent through the sample from the band-limited transducer to the receiver generating a focus of energy, an example of which is shown in Fig. 2(d). This chirp method both increases the total energy input to the system during the forward step and recognizes bandwidth limitations of transducers by utilizing a finite bandwidth source signal. The fundamental bandwidth is defined by the span of frequencies used in the chirp signal. Higher harmonic bands generated by nonlinear vibration are defined as integer multiples of the fundamental bandwidth.

Samples containing SCC in 304L stainless steel are created through exposure to a hot chemical bath.[61] Thirteen rods of length 12.7 cm (5 in) and diameter 1.59 cm (5/8 in) are cut in half along the length of the rod and then welded back together with a "V-groove" weld using 308 weld material, as shown in Fig. 3(a). One of the rods is left untouched while the remaining 12 rods are exposed to a 42% $MgCl_2$ bath at 80 °C [see Fig. 3(b)]. One rod is removed from the solution every two days, such that the shortest exposure time is two days and the longest is 24 days. An example of one of the rods exposed to $MgCl_2$ for 14 days is shown in Fig. 3(c), although SCC is not visually apparent. Water is added to the solution to maintain a consistent salinity as needed.

One at a time, a rod is epoxied to the top of a steel disk of diameter 20.2 cm (8 in) and height 2.5 cm (1 in), which is elevated by three rubber mounts 2 cm (0.79 in) above an optical table. Eight piezoelectric transducers are epoxied to the underside of the steel disk. Relative to the center of the disk, transducer 1's center is at a radius of 5.8 cm and located at 0°, transducer 2's center is at a radius of 5.3 cm and located at 34°, transducer 3's center is at a radius of 5.4 cm and located
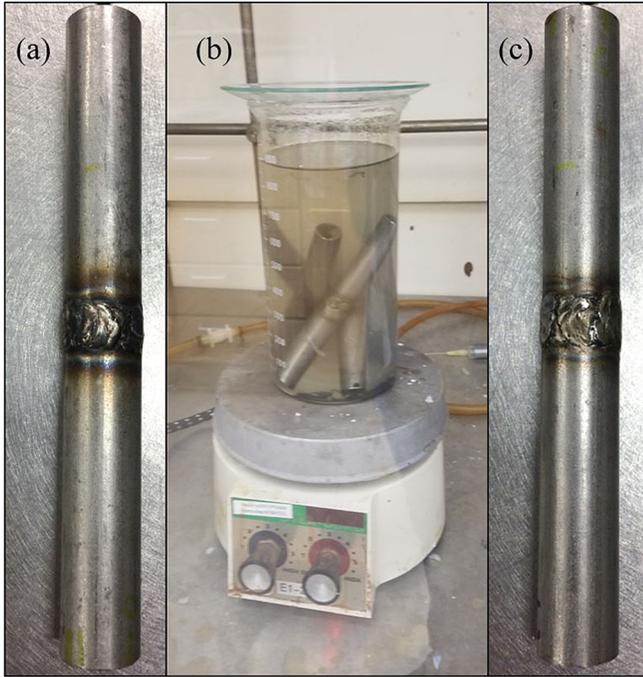
FIG. 3. (Color online) Photographs of the progression of rods from intact to damaged. (a) Undamaged 12.7 mm long, welded rod. The HAZ is evident in the discoloration. (b) Rods in the 42% solution of hot magnesium chloride (MgCl$_2$). (c) Damaged rod after 14 days exposure in the solution. The MgCl$_2$ bath removes much of the HAZ discoloration.
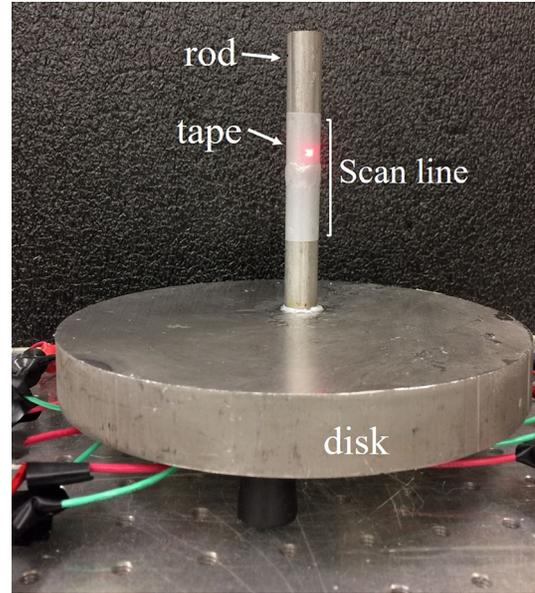

FIG. 4. (Color online) Photograph of the steel disk chaotic cavity with eight piezoelectric transducers epoxied to the underside. A rod under test is epoxied to the top of the disk and the laser light is visible on the upper half of the scale line just above the weld. The silver colored region on the rod is retro-reflective tape (simply labeled "tape" in the image) used to decrease optical noise. The scan line spans 25 mm above and below the center of the weld along the length of the rod.

at 74°, transducer 4's center is at a radius of 5.7 cm and located at 103°, transducer 5's center is at a radius of 5.5 cm and located at 158°, transducer 6's center is at a radius of 4.8 cm and located at 197°, transducer 7's center is at a radius of 4.1 cm and located at 252°, and transducer 8's center is at a radius of 5.2 cm and located at 291°. Because nonlinear increases to harmonic amplitudes can be difficult to detect without sufficiently high amplitude excitation, TR focusing from each of the eight transducers are simultaneously superposed to create a focus at a single location. Placing eight transducers on the rod itself is both inefficient given the curved rod surface and can physically block access to a cracked location. Therefore, the energy from the transducers is transmitted through the disk and into the rod. The disk creates a so called chaotic cavity to increase diffuse reverberation in the impulse responses.[62–64] The epoxy bond between the disk and rod is an average of 0.79 mm in thickness and care is taken to make the bond both consistent between rods and level such that the disk and rod do not have direct contact, thereby avoiding contact nonlinearity. The bond is given 36 h to cure before testing takes place. An image of a rod epoxied to the disk is shown in Fig. 4.

The nature of NDE of samples implies that the exact extent of any damage in the samples is truly unknown. While it is supposed that cracking will occur in the HAZ, the HAZ itself is a tenuously defined region, and damage could exist anywhere along the circumference of the rod. Thus a 50 mm scan is conducted along four lines of scan points with each line spaced apart by 90° angles around the rod. Between each measurement along a given scan line on a rod, the steel disk and sample setup is rotated by 90°. The SLDV

is positioned to provide very close to normal incidence sensing of surface vibration (along the length of the rod) throughout the scan.

During the forward propagation step, the chirp signal is broadcast from one source transducer at a time and the response is recorded by the SLDV at the current scan point. Each of the eight impulse responses between the eight source transducers and the current scan point are obtained as described previously. These impulse responses are reversed in time and amplified to the maximum output available from the amplifier. Each of the eight reversed impulse responses provides a TR focus at the current scan point that constructively interfere. The SLDV records the focal signal at this current scan point. The SLDV is then positioned at the next scan point and the entire process, described in this paragraph, is repeated. Thus, TR focusing occurs at the location where the SLDV is aimed during the forward propagation step.

III. RESULTS

Two focal signals are shown in Fig. 5 for illustrative purposes. Both of these signals come from the same rod exposed to MgCl$_2$ for 12 days and both are within the supposed HAZ, but Fig. 5(a) is the focal signal from a location 14.2 mm from the outer edge of the weld and Fig. 5(b) is only 2 mm from the weld. The first attribute of note, relative to many other TR experiments is the large temporal side lobes on either side of the peak focus.[65] While some applications of TR require a more delta-function like focal signal, this is less important for crack detection.[66] The high-amplitude side lobes in the focal signal imply that this system is a highly resonant one; in fact, spectral analysis suggests there are several sample resonance modes within

J. Acoust. Soc. Am. **145** (1), January 2019
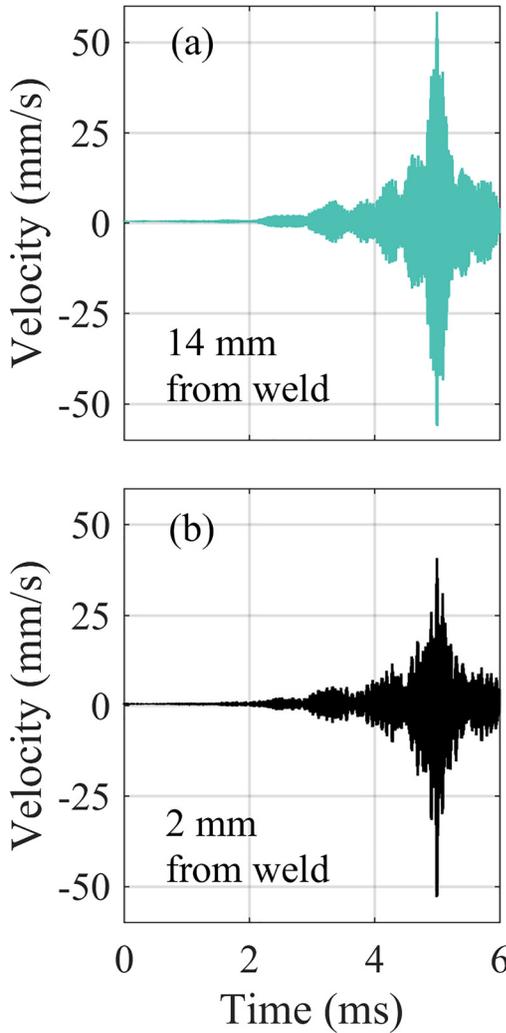
Young *et al.*   385

FIG. 5. (Color online) Time-domain focal signals from two scan points on the rod exposed to magnesium chloride for 12 days. (a) Focal signal 14.2 mm from the weld. (b) Focal signal 2 mm from the weld.

the frequency band used in the experiment.[59] The most important aspect of TR focusing for nonlinear detection is the amplitude of the signal, which triggers a nonlinear response and allows detection of nonlinear features (i.e., harmonics). Figure 6 shows the spatial distribution of the instantaneous velocity along the rod at the moment of a TR focus on an unexposed rod. The "×" symbol indicates the location of the focus as well as its amplitude at the focal-time. Examination of this figure indicates an average wavelength of 26 mm. Using the central excitation frequency of 100 kHz, the wave speed is calculated as 2600 m/s, a value close to the expected Rayleigh wave speed of 2860 m/s in 304L steel. TR inherently utilizes all types of propagating waves (i.e., propagation modes) present in a system. The authors expect that the waves used to generate focusing in the rod are likely dominated by antisymmetric (so called $A0$) lamb waves and torsional waves.

Potential nonlinearity in the focal signals, due to the presence of damage, is quantified from Fourier transforms of the signals in Fig. 5, shown in Fig. 7, and labeled with their distance from the outer edge of the weld. A comparison of the two signals on the same amplitude scale, shown in
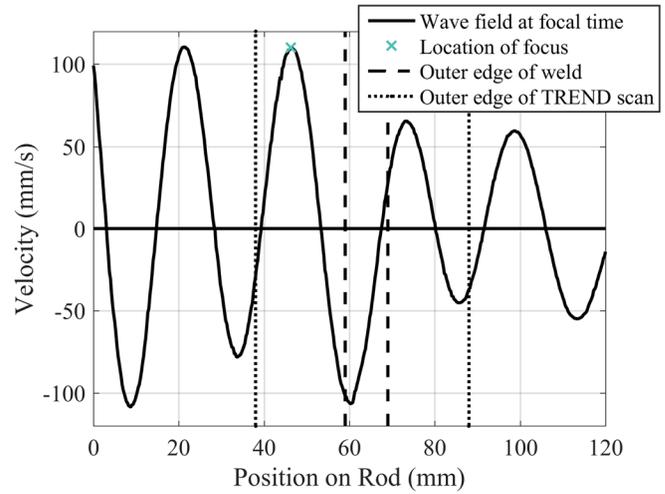

FIG. 6. (Color online) Instantaneous velocity along the length of rod at the moment of time reversal focusing on an unexposed rod. The focus is generated at the location marked by the ×.

Fig. 7, utilizes unnormalized spectra, $G(f)$, scaled according to the Euclidean norm of the values contained within the fundamental bandwidth

$$\|G(f)\| = \frac{G(f)}{\sqrt{\sum_{75\,\text{kHz}}^{125\,\text{kHz}} G^2(f)}}. \tag{1}$$

The fundamental bandwidth, outlined with vertical dashed-dotted lines in Fig. 7, is the same span of frequencies used for the chirp in the forward propagation step, from 75 to 125 kHz. This frequency band was selected because the transducers operate efficiently over this range. By scaling the spectra according to the norm of the fundamental bandwidth (the Euclidean norm), differences in focal amplitudes between spectra are removed, allowing any differences in higher harmonic content to be compared directly. The second harmonic, from
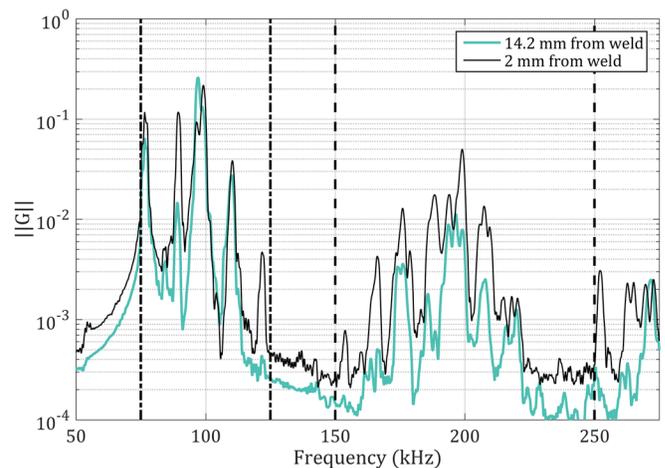

FIG. 7. (Color online) Spectra of the focal signals displayed in Fig. 5. Amplitude scaling to the Euclidean norm of the spectra within the fundamental bandwidth is applied, shown mathematically in Eq. (1). The fundamental bandwidth is outlined by the vertical dash-dot lines. The second harmonic is outlined by the vertical dashed lines.

150 to 250 kHz, is outlined in dashed vertical lines in Fig. 7 and comprises the region most likely to indicate the presence of nonlinearity introduced by crack motion. Other harmonics were examined but were buried in the noise floor. If the localized focus of energy excites SCC, the crack produces harmonics of the fundamental. The higher the amplitude of the spectra in the second harmonic relative to the fundamental amplitude, the larger extent of SCC is expected.[40] In Fig. 7, the two signals have approximately the same amplitude within the fundamental bandwidth, as expected given the applied scaling, although both have multiple peaks due to the resonances of the sample and source transducer. However, within the second harmonic band, the amplitudes for the spectrum corresponding to the location 2 mm from the weld are distinctly higher in amplitude than in the spectrum for the 14.2 mm distance from the weld, indicating a higher severity of damage. This result is expected given that SCC is more likely to form immediately adjacent to the boundary of the weld; nevertheless, both positions are within the HAZ and an examination of the entire spatial region is necessary to see the impact of a variety of differences in the second harmonic amplitude.

Nonlinearity across the entirety of a scan line is compared after the amplitude in the second harmonic is reduced to a single number. This is accomplished by calculating the scaled nonlinearity

$$\zeta(x, \theta_n) = \sum_{150\,\mathrm{kHz}}^{250\,\mathrm{kHz}} \|G(x, \theta_n, f)\|^2, \tag{2}$$

where the spectral amplitudes within the scaled second harmonic bandwidth are squared and summed for each scan point, x, and at the rotation angle, θ_n. The higher the scaled nonlinearity, the more likely SCC has developed at location (x, θ_n). The scaling of the focal spectra and comparison of relative amplitudes of the second harmonic is similar in nature to the frequency domain scaling subtraction method,[33,40] but the scaling

used here is based on the fundamental bandwidth of each spatial scan location rather than comparing a high-amplitude focal spectrum to a low-amplitude focal spectrum.

Scaled nonlinearity, $\zeta(x, \theta_n)$, results are shown in Fig. 8 for the rod exposed to $MgCl_2$ for 12 days. The four plots in Fig. 8 indicate the results from each of the four θ_{1-4} angles $0°$, $90°$, $180°$, and $270°$ in Figs. 8(a), 8(b), 8(c), and 8(d), respectively, scanned on the rod. The horizontal axis shows the scan position, x, in millimeters with distances relative to the top of the rod (the end not epoxied to the disk). The vertical axis displays the amplitude of $\zeta(x, \theta_n)$ and the vertical dashed lines indicate the location of the outer edges of the weld, at $x = 57$ and 68 mm. As anticipated, more nonlinearity exists either at or just outside the edge of the weld for all four angles. The highest amplitudes exist in Fig. 8(d), with the peak at 70 mm serving as the example signal in Fig. 5(b) and example spectrum in Fig. 7. While each of the four scans at each θ_n have clear peaks at the weld's edge, they also have distinct increases in nonlinearity elsewhere along the scan, as far as 15 mm ($x = 41$ mm) from the edge of the weld [see Fig. 8(a)] and even within the weld itself [Fig. 8(b)] The fact that SCC is likeliest to form just outside the weld does not restrict its growth to that region alone. In fact, it is impossible to nondestructively verify where tensioned grain boundaries or residual stresses exist, or even how far the HAZ extends from the edge of the weld. SCC can form in any location given the right conditions, so while the largest peaks in nonlinearity are expected to exist at the weld boundary, it is not surprising that other regions show peaks as well. Additionally, the weld region assumed for all four rotations was defined for one rotation angle θ and assumed to span the same positions for other θ_n.

Because the results depicted in Figs. 8(a)–8(d) all display peaks in $\zeta(x, \theta_n)$ just adjacent to the weld, it could be thought that what is detected is not nonlinearity from SCC at all, but merely odd behavior due to the edge of the weld. However, the data for the rod that was not exposed to the
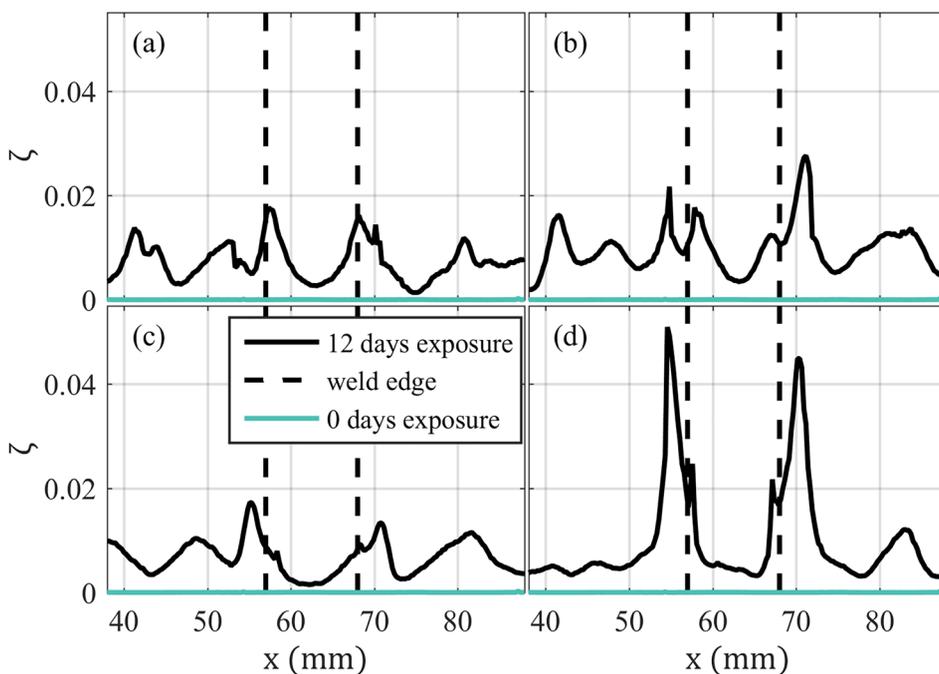
FIG. 8. (Color online) The scaled nonlinearity, $\zeta(x, \theta_n)$, in the second harmonic bandwidth, versus scan position, x (mm). Vertical dashed lines indicate the approximate outer edge of the weld. Data shown in black are from the rod exposed to the magnesium chloride bath for 12 days, while the curves in teal are for the rod exposed for zero days. Data are from a 200 point scan at (a) $0°$, (b) $90°$, (c) $180°$, and (d) $270°$.

MgCl$_2$ solution is also shown in each of these figures, and no spikes are observed at the edges of the welds in that sample. Some features exist at levels of $\zeta = 10^{-5}$ in the unexposed rod; however, these features are inconsistent spikes indicative of noise and occur at random locations on the rod, both near and far from the weld. Therefore, we assert that the nonlinearity detected in the exposed rods is due to SCC, and not the weld boundary.

NDE techniques utilize both linear and nonlinear metrics to detect damage. One might expect that severely damaged locations (open cracks) would possess high peak focal amplitude, as the excited crack is more freely able to vibrate at an open crack boundary than material constrained within a homogeneous medium. Thus, the fundamental bandwidth is expected to have higher amplitudes and the peak focal amplitude would be higher. In the research shown here, the two focal signals shown in Fig. 5 indicate that the rods not only constitute resonant systems, but that the highest focal amplitude did not correspond to the location where SCC is likely to exist, since the damaged location yielded a lower peak focal amplitude. Figure 9 illustrates the resonance characteristics of the rod more clearly by showing the peak focal amplitude, A_p, in mm/s of each independently generated focal signal on the left vertical axis plotted against x, and $\zeta(x, \theta_n)$ from the same data set on the right axis, also plotted versus x. The scan data are the same as that shown in Fig. 8(d). The peak focal amplitude ranges from 54 to 76 mm/s, and oscillates with an average peak to peak distance of 28 mm, a distance within 2 mm of the wavelength determined from the plot in Fig. 6. Notably, the peak focal amplitude is highest where $\zeta(x, \theta_n)$ is not. There is some indication that damage has an impact on focal amplitude, such as the matching peaks at $x = 54.6$, 57.6, and 67.2 mm. However, these minor peaks in focal amplitude are more likely to look like false detections than cracks if one were basing crack detection solely on the peak focal amplitude, when comparing those minor peaks to the large amplitude gains at $x = 48$, 62, and 76 mm. While an increase in peak focal amplitude may be a valuable linear indicator of

damage for some varieties of cracking, it is apparently not sufficient for SCC in a resonant system, and could lead to erroneous results. This result indicates the importance of NDE imaging based on nonlinearities generated by cracking. In addition, given the wavelength of 26 mm, the defects should only be detected if they are larger than the half-wavelength diffraction limit of 13 mm. However, nonlinear cracking features appear to be discernable in regions as small as 5 mm. Though beyond the scope of this paper, this could be the result of the diffraction limit of the second harmonic used, approximately 6 mm.

Of the 12 rods exposed to MgCl$_2$, ten showed evidence of nonlinearity in the HAZ, especially adjacent to the weld. The two that did not were only exposed for two days and four days. To compare the total damage in the rods, all of the localized and scaled nonlinearity ($\zeta(x, \theta_n)$) like that shown in Fig. 8 must be quantified for each rod. Because each focal spectra is scaled to the amplitude of its fundamental bandwidth, differences in focal amplitude (which is dominated by the fundamental frequency bandwidth) between the rods has no impact and only the relative height of the second harmonic, the scaled nonlinearity, is used as a damage indicator. The entire length of the scan is used to quantify a total nonlinearity for each rod because, as was evident in Fig. 8, not all spikes in $\zeta(x, \theta_n)$ occur adjacent to the weld, and all nonlinearity should be accounted for. To determine the total nonlinearity, $Z(\theta_n)$, for each rotation angle on each rod, the $\zeta(x, \theta_n)$ values for each of the 200-point scans are averaged

$$Z(\theta_n) = \sqrt{\frac{1}{200} \sum_{n=1}^{200} \zeta(n, \theta_n)}. \tag{3}$$

The values at each angle $\theta_1, \theta_2, \theta_3, \theta_4 = 0°, 90°, 180°, 270°$ are then averaged to determine one value of total nonlinearity for each rod, Z

$$Z = \sqrt{\frac{1}{4 \times 200} \sum_{\theta_{n=1}}^{\theta_4} \sum_{n=1}^{200} \zeta(n, \theta_n)}.$$

Z, along with the four $Z(\theta_n)$ values, are plotted versus the amount of time each rod is exposed to the hot MgCl$_2$ solution in Fig. 10. The rods exposed from zero to four days have total nonlinearity values that are very low and essentially negligible. For the rods exposed from six to 24 days, various amounts of nonlinearity are detectable and there is an overall increase in Z with exposure time. Notable exceptions to this trend are the rods exposed for 10, 16, and 20 days, which show surprisingly low Z given their exposure time. However, because welding is not an exact process, it is not known whether these rods had very little residual stress compared to their peers in the regions examined. It is also possible that the four angles examined on these rods simply missed whatever SCC was present within the rods. Studying a larger set of samples would determine the expected amount of variance in this trend of Z versus exposure time. The data is erratic particularly from the sample exposed for 14 days to the sample exposed for 20 days. However, the general
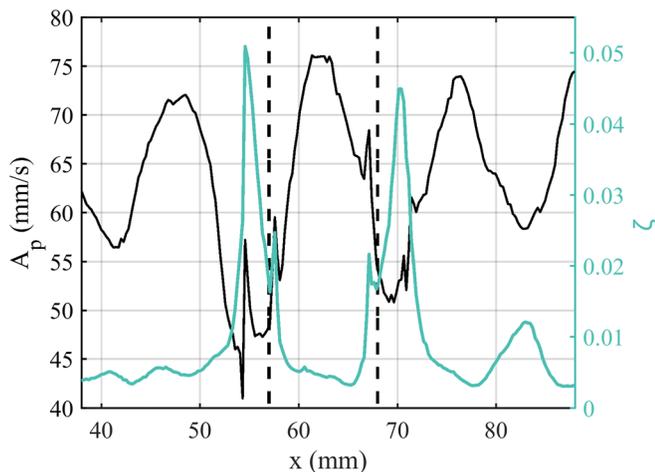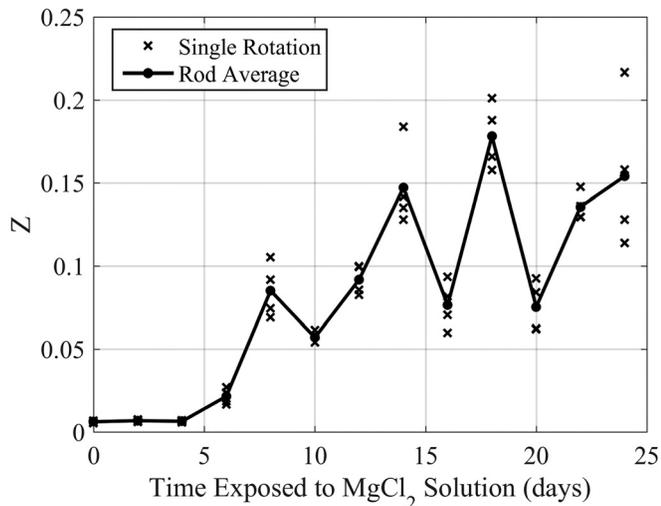

FIG. 9. (Color online) Left axis: peak focal amplitude, A_p, versus scan position, x. Right axis: scaled nonlinearity, $\zeta(x, \theta_n)$, versus scan position. The outer edges of the weld are indicated by the vertical dashed lines.

FIG. 10. Total nonlinearity, Z, measured in each rod versus the amount of time the rod was exposed to the hot solution of magnesium chloride ($MgCl_2$). The nonlinearity measured for each rotation is given by the $\times$ symbols and Z is denoted by the solid circles and represents an average of the four rotations.

increase in Z with exposure time suggests that TREND can be used to track SCC progression over time on similar samples and need not be a measurement system limited to measurements on a single sample. Given this result, TREND could be utilized on storage casks to determine the extent of SCC growth. However, the nonlinearity observed over the short exposure times used here would not be expected to translate to actual casks because the corrosive environment for storage casks is not nearly as severe.

It is worth noting that a parallel study was conducted by Hogg et al.[67] (many of the authors of this paper) using nonlinear resonant ultrasound spectroscopy on these same samples to measure the amplitude dependent frequency shift of the fundamental longitudinal mode in the samples. These results also did not show any significant increase in the measured nonlinearity in the virgin sample and the samples exposed for two and four days. The samples exposed for longer time generally showed an increase in nonlinearity with increasing exposure time; however, the samples exposed for 10 and 20 days each had significantly lower measured nonlinearity in them as would determined in the present paper. The sample exposed for 16 days also showed a significant drop in Z in this paper, but a similar drop was not observed by Hogg et al.

IV. CONCLUSION

Thirteen stainless steel rods were cut in half and welded back together and exposed to a solution of hot magnesium chloride for varying amounts of time. Using TREND, each of the rods was scanned, placing a high-amplitude focus of energy at each scan location, and the nonlinear content in the second harmonic was quantified in the scaled focal signals. It was found that the focal signals of scan points adjacent to the outer edge of the weld overall contained more nonlinearity, an expected result given the propensity of these regions to SCC being located within the heat-affected zone.

Additionally, the maxima of the focal signals, a linear imaging quantity, at each scan location could not be used to identify locations with SCC. A value for total nonlinearity was quantified for each rod, and it was found that, in general, the longer a rod was exposed to the hot solution of magnesium chloride, the more nonlinearity was detected. Thus, this paper illustrated that SCC around welds can not only be detected using TREND, but the nonlinear signature measured with TREND increases with the expected amount of SCC from longer exposure to corrosive environments.

[1]M. Fink, "Time reversed acoustics," Phys. Today **50**(3), 34–40 (1997).

[2]B. E. Anderson, M. Griffa, C. Larmat, T. J. Ulrich, and P. A. Johnson, "Time reversal," Acoust. Today **4**(1), 5–16 (2008).

[3]C. Heaton, B. E. Anderson, and S. M. Young, "Time reversal focusing of elastic waves in plates for educational demonstration purposes," J. Acoust. Soc. Am. **141**(2), 1084–1092 (2017).

[4]M. Scalerandi, A. S. Gliozzi, C. L. E. Bruno, D. Masera, and P. Bocca, "A scaling method to enhance detection of a nonlinear elastic response," Appl. Phys. Lett. **92**(10), 101912 (2008).

[5]M. Scalerandi, A. S. Gliozzi, C. L. E. Bruno, and K. Van Den Abeele, "Nonlinear acoustic time reversal imaging using the scaling subtraction method," J. Physics D: Appl. Phys. **41**(21), 215404 (2008).

[6]A. Sutin, P. Johnson, and J. TenCate, "Development of nonlinear time reverse acoustics (NLTRA) for application to crack detection in solids," in Proceedings of the 5th World Congress on Ultrasonics, Paris, France (September 7–10, 2003), pp. 121–124.

[7]A. M. Sutin, J. A. TenCate, and P. A. Johnson, "Single-channel time reversal in elastic solids," J. Acoust. Soc. Am. **116**(5), 2779–2784 (2004).

[8]N. Chakroun, M. Fink, and F. Wu, "Ultrasonic nondestructive testing with time reversal mirrors," in Proceedings of the IEEE Ultrasonics Symposium, Tucson, AZ (October 20–23, 1992), pp. 809–814.

[9]N. Chakroun, M. Fink, and F. Wu, "Time reversal processing in ultrasonic nondestructive testing," IEEE Trans. Ultrason. Ferroelectr. Freq. Control **42**, 1087–1098 (1995).

[10]V. Miette, L. Sandrin, F. Wu, and M. Fink, "Optimisation of time reversal processing in titanium inspections," in Proceedings of the 1996 IEEE Ultrasonics Symposium, San Antonio, TX (November 3–6, 1996), pp. 643–647.

[11]R. K. Ing and M. Fink, "Time recompression of dispersive Lamb wave using a time reversal mirror. Applications to flaw detection in thin plates," Proceedings of the 1996 IEEE Ultrasonics Symposium, San Antonio, TX (November 3–6, 1996), pp. 659–664.

[12]C. Prada and M. Fink, "Separation of interfering acoustic scattered signals using the invariant of the time-reversal operator. Application to Lamb waves characterization," J. Acoust. Soc. Am. **104**, 801–807 (1998).

[13]E. Kerbrat, R. K. Ing, C. Prada, D. Cassereau, and M. Fink, "The DORT method applied to detection and imaging in plates using Lamb waves," AIP Conf. Proc. **557**, 934 (2001).

[14]C. Prada, E. Kerbrat, D. Cassereau, and M. Fink, "Time reversal techniques in ultrasonic nondestructive testing of scattering media," Inv. Prob. **18**, 1761–1773 (2002).

[15]E. Kerbrat, C. Prada, D. Cassereau, and M. Fink, "Ultrasonic nondestructive testing of scattering media using the decomposition of the time reversal operator," IEEE Trans. Ultrason. Ferroelectr. Freq. Control. **49**, 1103–1113 (2002).

[16]C. Prada, F. Wu, and M. Fink, "The iterative time reversal mirror: A solution to self-focusing in the pulse-echo mode," J. Acoust. Soc. Am. **90**(2), 1119–1129 (1991).

[17]C. Prada, J-L. Thomas, and M. Fink, "The iterative time reversal process: Analysis of the convergence," J. Acoust. Soc. Am. **97**(1), 62–71 (1995).

[18]E. H. Saenger, G. K. Kocur, R. Judd, and M. Torrilhon, "Application of time reverse modeling on ultrasonic nondestructive testing of concrete," Appl. Math. Model. **35**(2), 807–816 (2011).

[19]J. Douma, E. Niederleithinger, and R. Snieder, "Locating events using time reversal and deconvolution: Experimental application and analysis," J. Nondestruct. Eval. **34**, 2 (2015).

[20]C. Larmat, J.-P. Montagner, M. Fink, Y. Capdeville, A. Tourin, and E. Clevede, "Time-reversal imaging of seismic sources and applications to the great Sumatra earthquake," Geophys. Res. Lett. **33**(19), L19312, https://doi.org/10.1029/2006GL026336 (2006).

[21]C. Larmat, J. Tromp, Q. Liu, and J.-P. Montagner, "Time-reversal location of glacial earthquakes," J. Geophys. Res. **113**(B9), B09314, https://doi.org/10.1029/2008JB005607 (2008).

[22]C. Larmat, R. A. Guyer, and P. A. Johnson, "Tremor source location using time-reversal: Selecting the appropriate imaging field," Geophys. Res. Lett. **36**(22), L22304, https://doi.org/10.1029/2009GL040099 (2009).

[23]C. S. Larmat, R. A. Guyer, and P. A. Johnson, "Time-reversal methods in geophysics," Phys. Today **63**(8), 31–35 (2010).

[24]R. K. Ing and N. Quieffin, "In solid localization of finger impacts using acoustic time-reversal process," Appl. Phys. Lett. **87**(20), 204104 (2005).

[25]D. Vigoureux and J.-L. Guyader, "A simplified time reversal method used to localize vibrations sources in a complex structure," Appl. Acoust. **73**(5), 491–496 (2012).

[26]C. Fan, M. Pan, F. Luo, and B. W. Drinkwater, "Multi-frequency time-reversal-based imaging for ultrasonic nondestructive evaluation using full matrix capture," IEEE Trans. Ultrason. **61**(12) 2067–2074 (2014).

[27]C. Fan, M. Caleap, M. Pan, and B. W. Drinkwater, "A comparison between ultrasonic array beamforming and super resolution imaging algorithms for non-destructive evaluation," Ultrasonics **54**, 1842–1850 (2014).

[28]G. Zhao, D. Zhang, L. Zhang, and B. Wang, "Detection of defects in reinforced concrete structures using ultrasonic nondestructive evaluation with piezoelectric transducers and the time reversal method," Sensors **18**(12), 4176 (2018).

[29]R. Guyer, "Nonlinear tomography and time reversed acoustics," in *Proceedings of the 6th International Workshop on Nonlinear Elasticity in Materials*, Leuven, Belgium (June 18–22, 2001).

[30]P. P. Delsanto, P. A. Johnson, M. Scalerandi, and J. A. TenCate, "LISA simulations of time-reversed acoustic and elastic wave experiments," J. Phys. D: Appl. Phys. **35**(23), 3145–3152 (2002).

[31]O. Bou Matar, S. Dos Santos, J. Fortineau, T. Goursolle, L. Haumesser, and F. Vander Meulen, "Pseudo spectral simulations of elastic waves propagation in heterogeneous nonlinear hysteretic medium," in *Proceedings of the 17th International Symposium on Nonlinear Acoustics*, State College, PA (July 18–22, 2005), pp. 95–98.

[32]T. J. Ulrich, P. A. Johnson, and A. Sutin, "Imaging nonlinear scatterers applying the time reversal mirror," J. Acoust. Soc. Am. **119**(3), 1514–1518 (2006).

[33]P.-Y. Le Bas, M. C. Remillieux, L. Pieczonka, J. A. Ten Cate, B. E. Anderson, and T. J. Ulrich, "Damage imaging in a laminated composite plate using an air-coupled time reversal mirror," Appl. Phys. Lett. **107**, 184102 (2015).

[34]T. J. Ulrich, P. A. Johnson, and R. A. Guyer, "Interaction dynamics of elastic waves with a complex nonlinear scatterer through the use of a time reversal mirror," Phys. Rev. Lett. **98**, 104301 (2007).

[35]T. J. Ulrich, A. M. Sutin, T. Claytor, P. Papin, P.-Y. Le Bas, and J. A. TenCate, "The time reversed elastic nonlinearity diagnostic applied to evaluation of diffusion bonds," Appl. Phys. Lett. **93**(15), 151914 (2008).

[36]P.-Y. Le Bas, T. J. Ulrich, B. E. Anderson, R. A. Guyer, and P. A. Johnson, "Probing the interior of a solid volume with time reversal and nonlinear elastic wave spectroscopy," J. Acoust. Soc. Am. **130**(4), EL258–EL263 (2011).

[37]B. E. Anderson, M. Griffa, T. J. Ulrich, P.-Y. Le Bas, R. A. Guyer, and P. A. Johnson, "Crack localization and characterization in solid media using time reversal techniques," in *Proceedings of the 44th U.S. Rock Mechanics Symposium and 5th U.S.-Canada Rock Mechanics Symposium*, Salt Lake City, Utah (June 27–30, 2010), Paper No. #10-154.

[38]B. E. Anderson, M. Griffa, P.-Y. Le Bas, T. J. Ulrich, and P. A. Johnson, "Experimental implementation of reverse time migration for nondestructive evaluation applications," J. Acoust. Soc. Am. **129**(1), EL8–EL14 (2011).

[39]P. Blanloeuil, L. R. F. Rose, J. A. Guinto, M. Veidt, and C. H. Wang, "Closed crack imaging using time reversal method based on fundamental and second harmonic scattering," Wave Motion **66**, 156–176 (2016).

[40]B. E. Anderson, L. Pieczonka, M. C. Remillieux, T. J. Ulrich, and P.-Y. Le Bas, "Stress corrosion crack depth investigation using the time reversed elastic nonlinearity diagnostic," J. Acoust. Soc. Am. **141**(1), EL76–EL81 (2017).

[41]G. Zumpano and M. Meo, "A new nonlinear elastic time reversal acoustic method for the identification and localisation of stress corrosion cracking in welded plate-like structures—A simulation study," Int. J. Solids Struct. **44**(11), 3666–3684 (2007).

[42]M. C. Remillieux, P.-Y. Le Bas, L. Pieczonka, B. E. Anderson, and T. J. Ulrich, "Estimating the penetration depth and orientation of stress corrosion cracks using time-reversal acoustics," Trans. Am. Nuclear Soc. **115**, 217–220 (2016).

[43]B. E. Anderson, M. C. Remillieux, P.-Y. Le Bas, and T. J. Ulrich, "Time reversal techniques," in *Nonlinear Acoustic Techniques for Nondestructive Evaluation*, 1st ed., edited by T. Kundu, (Springer and Acoustical Society of America, New York, 2018), Chap. 14, pp. 547–581.

[44]P. B. Nagy, "Fatigue damage assessment by nonlinear ultrasonic materials characterization," Ultrasonics **36**, 375–381 (1998).

[45]T. J. Ulrich, B. E. Anderson, M. C. Remillieux, P. Y. Le Bas, and L. Pieczonka, "Application of nonlinear ultrasonics to inspection of stainless steel for dry storage," Technical Report No. LA-UR-15-27382, Los Alamos National Laboratory (LANL), Los Alamos, NM, 2015.

[46]E. Gray, "Coast to coast spent fuel dry storage problems and recommendations," in *Proceedings of the Division of Spent Fuel Management Regulatory Conference*, Rockville, MD (November 18–19, 2015), http://www.nrc.gov/public-involve/conferencesymposia/dsfm/2015/dsfm-2015-erica-gray.pdf (Last viewed June 7, 2018).

[47]K. L. Banovac, "Summary of August 5, 2014, public meeting with the nuclear energy institute on chloride induced stress corrosion cracking regulatory issue resolution protocol," U.S. Nuclear Regulatory Commission Public Meeting (August 2014), http://pbadupws.nrc.gov/docs/ML1425/ML14258A081.pdf (Last viewed June 7, 2018).

[48]D. S. Dunn, "Chloride-induced stress corrosion cracking tests and example aging management program," U.S. Nuclear Regulatory Commission Public Meeting (August 2014), https://www.nrc.gov/docs/ML1425/ML14258A082.pdf (Last viewed June 7, 2018).

[49]A. O'Brien, *Welding Handbook* (American Welding Society, Miami, FL, 2011), Vol. 4, pp. 308–313.

[50]A. Bustreo, "All you need to know about the heat-affected zone," in The Fabricator (July 2016), https://www.thefabricator.com/article/shopmanagement/all-you-need-to-know-about-the-heat-affected-zone (Last viewed on June 7, 2018).

[51]C. L. Jenney and A. O'Brien, *Welding Handbook* (American Welding Society, Miami, FL, 2001), Vol. 1, pp. 136.

[52]Y. Ohara, H. Endo, T. Mihara, and K. Yamanaka, "Ultrasonic measurement of closed stress corrosion crack depth using subharmonic phased array," Jpn. J. Appl. Phys. **48**(7S), 07GD01 (2009).

[53]A. Ouchi, A. Sugawara, Y. Ohara, and K. Yamanaka, "Subharmonic phase array for crack evaluation using surface acoustic wave," Jpn. J. Appl. Phys. **54**(7S1), 07HC05 (2015).

[54]J. Riviere, M. Remillieux, Y. Ohara, B. E. Anderson, S. Haupert, T. J. Ulrich, and P. A. Johnson, "Dynamic acousto-elasticity in a fatigue-cracked sample," J. Nondestruct. Eval. **33**(2), 216–225 (2014).

[55]Y. Ohara, B. E. Anderson, T. J. Ulrich, P.-Y. Le Bas, P. A. Johnson, and S. Haupert, "Localization of closed cracks using multi-mode nonlinear resonant ultrasound spectroscopy," J. Jpn. Soc. Nondest. Inspec. **64**(12), 571–578 (2015).

[56]F. Morlock, L. J. Jacobs, J.-Y. Kim, P. Singh, and J. J. Wall, "Nonlinear ultrasonic assessment of stress corrosion cracking damage in sensitized 304 stainless steel," AIP Conf. Proc. **1650**, 1641–1647 (2015).

[57]A. Parvulescu, "Signal detection in a multipath medium by M. E. S. S. processing," J. Acoust. Soc. Am. **33**(11), 1674 (1961).

[58]A. Parvulescu and C. S. Clay, "Reproducibility of signal transmission in the ocean," Radio Electr. Eng. **29**, 223–228 (1965).

[59]B. Van Damme, K. Van Den Abeele, Y. Li, and O. Bou Matar, "Time reversed acoustics techniques for elastic imaging in reverberant and nonreverberant media: An experimental study of the chaotic cavity transducer concept," J. Appl. Phys. **109**, 104910 (2011).

[60]B. E. Anderson, M. Clemens, and M. L. Willardson, "The effect of transducer directionality on time reversal focusing," J. Acoust. Soc. Am. **142**(1), EL95–El101 (2017).

[61]B. K. Jackson, D. A. Bosko, M. T. Cronin, J. L. W. Warwick, and J. J. Wall, "Detection of incipient SCC damage in primary loop piping using fiber optic strain gages," in *ASME 2014 Pressure Vessels and Piping Conference*, Anaheim, CA (July 20–24, 2014), PVP2014-28979.

[62]G., Montaldo, D. Palacio, M. Tanter, and M. Fink, "Time reversal kaleidoscope: A smart transducer for three-dimensional ultrasonic imaging," Appl. Phys. Lett. **84**(19), 3879–3881 (2004).

[63]O. Bou Matar, Y. F. Li, and K. Van Den Abeele, "On the use of a chaotic cavity transducer in nonlinear elastic imaging," Appl. Phys. Lett. **95**, 141913 (2009).

[64]S. Delrue, K. Van Den Abeele, and O. Bou Matar, "Simulation study of a chaotic cavity transducer based virtual phased array used for focusing in the bulk of a solid material," Ultrasonics **67**, 151–159 (2016).

[65]C. Draeger, J-C. Aime, and M. Fink, "One-channel time reversal in chaotic cavities: Experimental results," J. Acoust. Soc. Am. **105**(2), 618–625 (1999).

[66]B. E. Anderson, J. Douma, T. J. Ulrich, and R. Snieder, "Improving spatio-temporal focusing and source reconstruction through deconvolution," Wave Motion **52**(9), 151–159 (2015).

[67]S. M. Hogg, B. E. Anderson, P.-Y. Le Bas, and M. C. Remillieux, "Nonlinear resonant ultrasound spectroscopy of stress corrosion cracking in stainless steel rods," NDT&E Int. **102**, 194–198 (2019).

J. Acoust. Soc. Am. **145** (1), January 2019

Young *et al.* 391